Electronic Supplementary Information

Highly stable multifunctional aptamer for enhancing antitumor immunity to against hepatocellular carcinoma by blocking dual immune checkpoint

Yanlin Du,[a,b,c,#] Da Zhang,[a,#] Yiru Wang,[d] Ming Wu,[a] Cuilin Zhang,[a] Youshi Zheng,[a] Aixian Zheng,[a,*] Xiaolong Liu[a,b*]

[a]The United Innovation of Mengchao Hepatobiliary Technology Key Laboratory of Fujian Province, Mengchao Hepatobiliary Hospital of Fujian Medical University, Fuzhou 350025, P. R. China;
[b]Fujian Institute of Research on The Structure of Matter, Chinese Academy of Sciences, Fuzhou 350002, P. R. China;
[c]College of Life Science, Fujian Agriculture and Forestry University, Fuzhou 350002, P. R. China;
[d]College of Biological Science and Engineering, Fuzhou University, Fuzhou 350116, P. R. China.

#These authors contributed equally to this work.

*Corresponding authors. E-mail: zax040500273@126.com; xiaoloong.liu@gmail.com

PD-L1-apt	ACGGGCCACATCAACTCATTGATAGACAATGCGTCC ACTGCCCGT
CTLA-4-apt	TCCCTACGGCGCTAACGATGGTGAAAATGGGCCTAGGG TGGACGGTGCCACCGTGCTACAAC
P1/C4-bi-apt	5'P_GAGACGGGCCACATCAACTCATTGATAGACAATGCG TCCACTGCCCGTCTCGCTCAGGTTCCCTACGGCGCTAA CGATGGTGAAAATGGGCCTAGGGTGGACGGTGCCACC GTGCTACAACACCTGAGC-3'OH
P1-apt	5'P_GAGACGGGCCACATCAACTCATTGATAGACAATGCG TCCACTGCCCGTCTCGCTCAGGTAAAAAAAAAAAAAAAA AAAAAAAAAAAAAAAAAAAAAAAAAAAAAAAAAAAAAAAA AAAAAAACCTGAGC-3'OH
C4-apt	5'P_GAGACGGGCAAAAAAAAAAAAAAAAAAAAAAAAAA AAAAAAGCCCGTCTCGCTCAGGTTCCCTACGGCGCTAA CGATGGTGAAAATGGGCCTAGGGTGGACGGTGCCACC GTGCTACAACACCTGAGC-3'OH

Table S1. The sequences of the oligonucleotides used in this paper. The letters in red represent the auxiliary sequences at the junction of PD-L1 aptamer and CTLA-4 aptamer to form a gapped double-stranded bridge structure. P1-apt and C4-apt were utilized as control aptamers that can bind to PD-L1-positive tumor cells and CTLA-4-positive T cells, respectively.

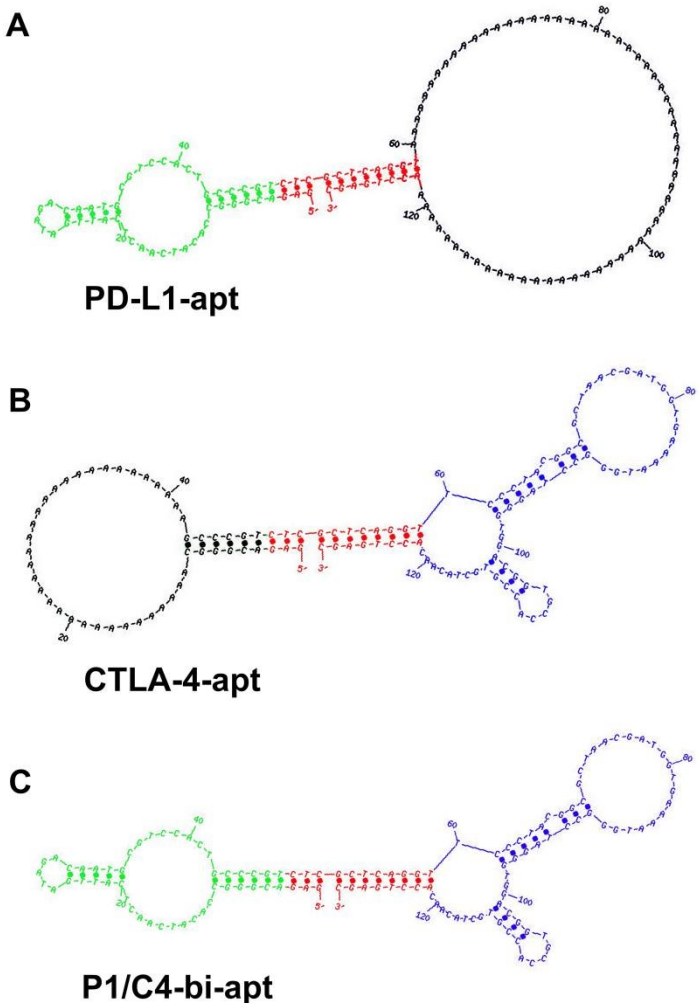

Fig. S1. The predicted structures of the oligonucleotides used in this paper. The letters in green represent the sequences of PD-L1 aptamer, and the letters in blue represent the sequences of CTLA-4 aptamer.

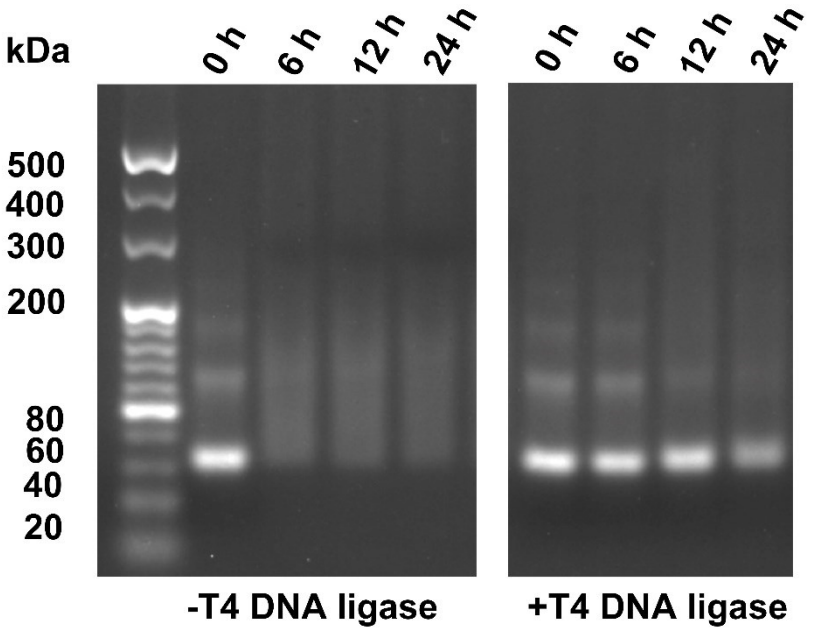

Fig. S2. The stability of P1/C4-bi-apt in murine serum. 2% agarose gel electrophoresis determination of (left) uncyclized P1/C4-bi-apt and (right) cyclized P1/C4-bi-apt dispersed in 10% murine serum at 37 ℃ for 0 h, 6 h, 12 h and 24 h.

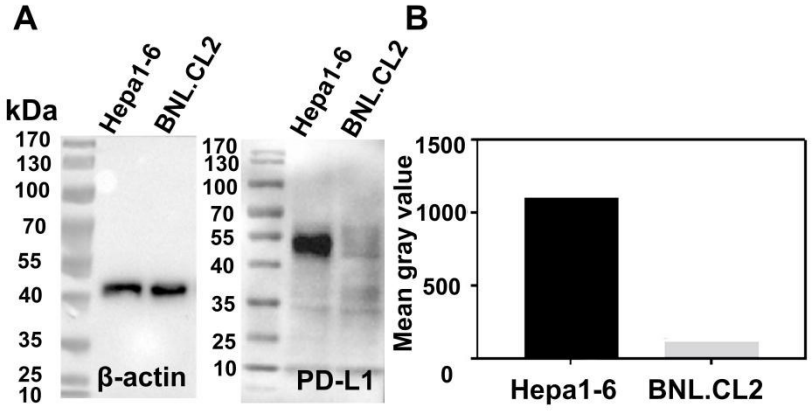

Fig. S3. The PD-L1 expression of different cell lines. (A) The expression of PD-L1 on Hepa1-6 cells and BNL.CL2 cells determined by Western blot. (B) Quantification of PD-L1 expression of Hepa1-6 cells and BNL.CL2 cells by using Image J.

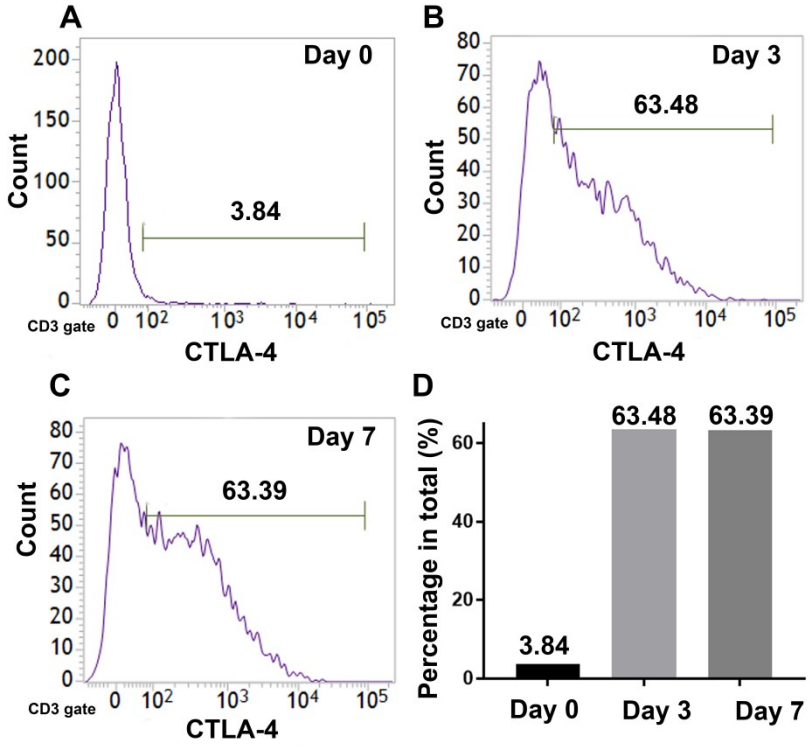

Fig. S4. The proportion of CTLA-4-positive T cells in activated PBMCs. (A) Representative FACS gating strategy for detecting the percentage of CTLA-4-positive cells in non-activated T cells (without anti-CD3/CD28 antibody activation), which are gated on $CD3^+$ T cells. The percentage of CTLA-4-positive cells in T cells at 3 days (B) and 7 days (C) post-activation. The above data are all gated on $CD3^+$ T cells. (D) The percentage of CTLA-4 at different time in total cells, analyzed by flow cytometry.

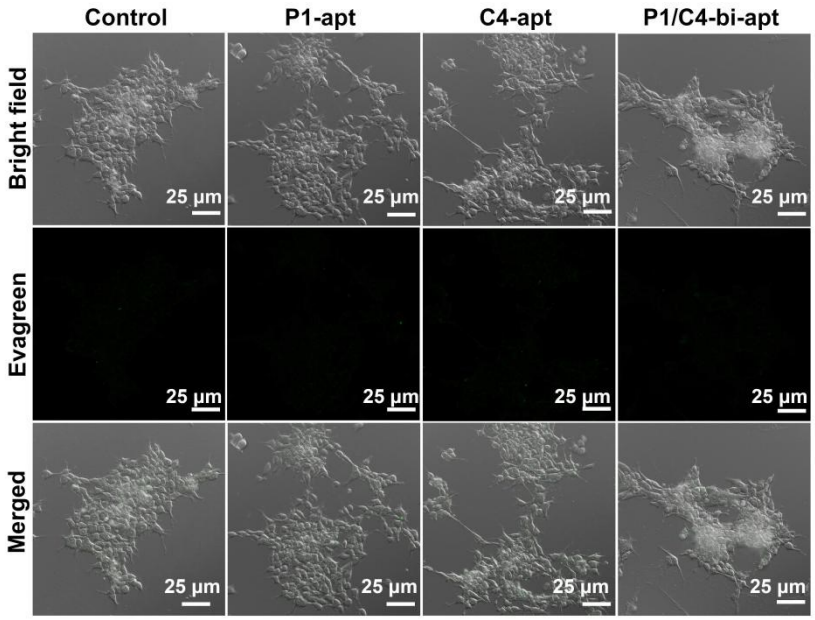

Fig. S5. The binding ability of different aptamers to PD-L1 low-expressed BNL.CL2 cell line. Confocal laser scanning microscopy (CLSM) images of BNL.CL2 cells incubated with Evagreen labeled P1-apt, C4-apt or P1/C4-bi-apt. BNL.CL2 cells without any treatment were experimented as control. Scale bar, 50 μm. (Evagreen excited by 488 nm)

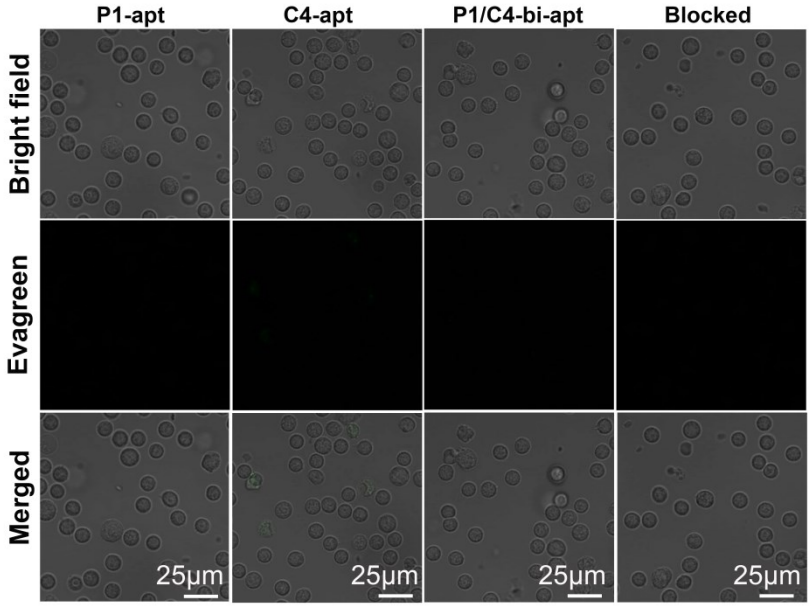

Fig. S6. The binding ability of different aptamers to CTLA-4-negative T cells. Confocal laser scanning microscopy (CLSM) images of T cells incubated with Evagreen labeled P1-apt, C4-apt, P1/C4-bi-apt or pretreated with anti-CTLA-4 antibody before added with P1/C4-bi-apt. Scale bar, 25 μm. (Evagreen excited by 488 nm)

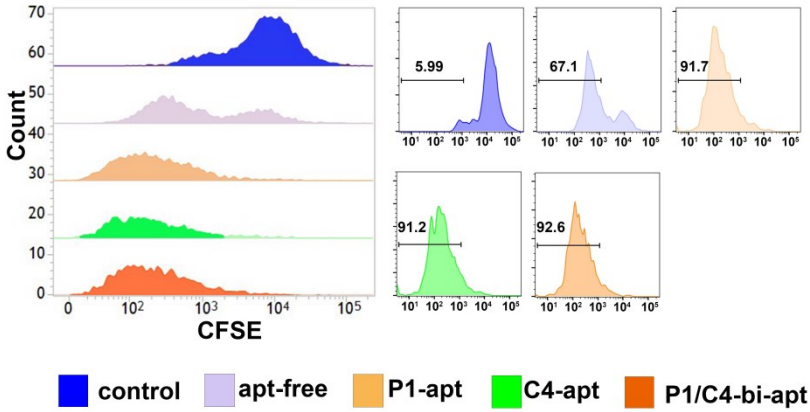

Fig. S7. Proliferation of mouse lymphocytes measured by CFSE assay. Flow cytometry analysis of CFSE-labeled allogeneic mouse lymphocytes after 72 h treatments (aptamer-free, P1-apt, C4-apt and P1/C4-bi-apt). The cells without any treatment were experimented as control. CFSE intensity was measured by flow cytometry on the gated $CD3^+$ population.

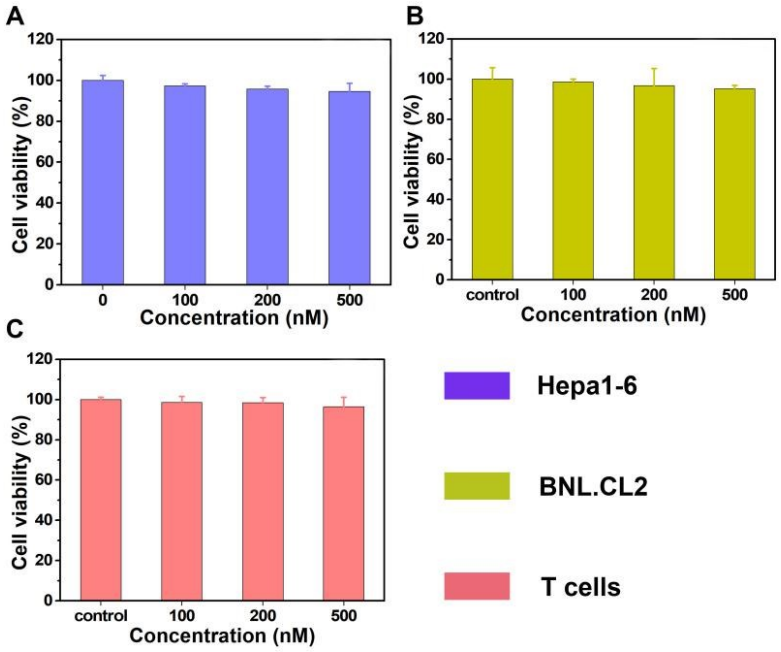

Fig. S8. Cytotoxicity evaluation of P1/C4-bi-apt by CCK-8 assay. Different cell lines including Hepa1-6 (tumor cell line) (A), BNL.CL2 (normal cell line) (B) and T cells (C) were treated with varying concentration of P1/C4-bi-apt for 24 h, and cell viability was detected with CCK-8. The results are the mean ± SD (n = 5).

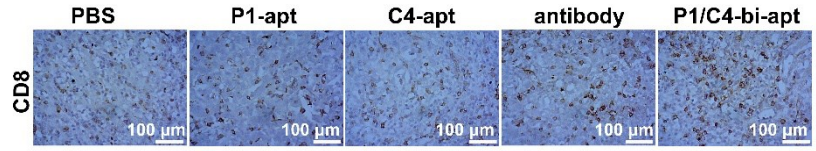

Fig. S9. The tumor-infiltrating T lymphocytes in tumors of different groups. Immunohistochemistry staining of tumor tissue slices to analyze the tumor-infiltrating lymphocytes, as determined by optical microscope. Scar bar is 100 μm.

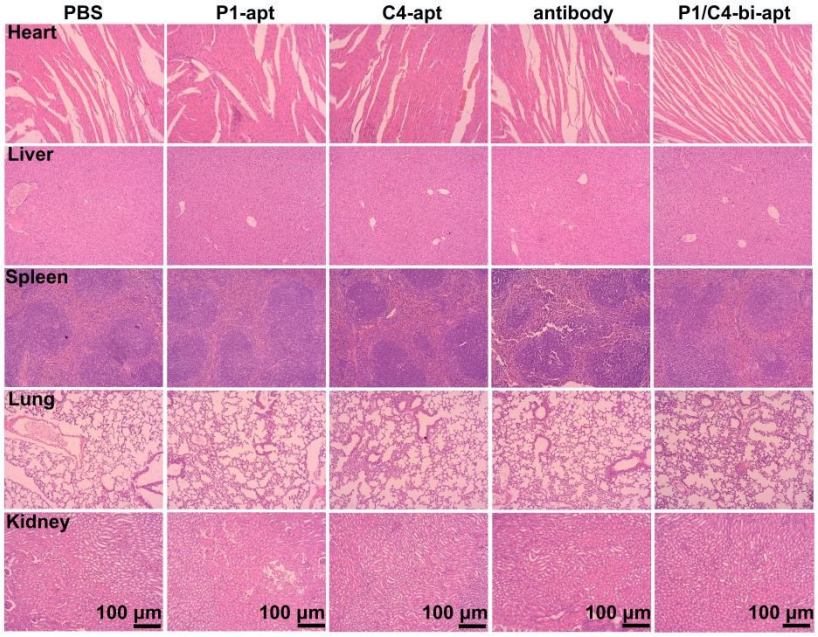

Fig. S10. Immunohistochemical analysis of major organs in tumor-bearing mice. Pathological changes in major organs (heart, liver, spleen, lung, kidney) evaluated by H&E staining at 3 days post-last treatment. Scar bar is 100 μm.

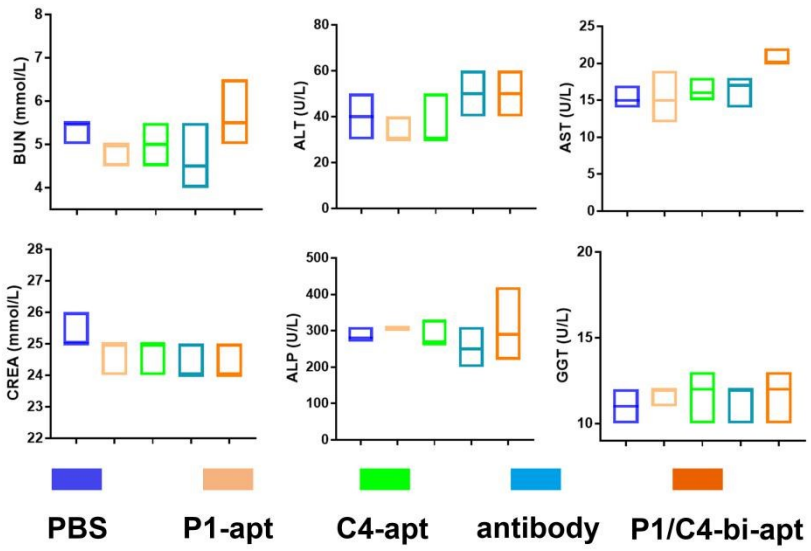

Fig. S11. Serum biochemical indicators of tumor-bearing mice after different treatment. Blood biochemistry analysis of liver, kidney and cardiac function markers after intravenous injection with PBS, P1-apt, C4-apt, anti-PD-L1 antibody and P1/C4-bi-apt. Data are present as the mean ± SD (n = 3).